BIOPHYSICS

Unveiling long-range forces in light-harvesting proteins: Pivotal roles of temperature and light

Elsa Perez-Martin[1]†, Tristan Beranger[1]†, Laurent Bonnet[2]†, Frederic Teppe[2], Alvydas Lisauskas[3], Kestutis Ikamas[3], Elwin Vrouwe[4], Elena Floriani[5], Gergely Katona[6], Didier Marguet[7], Vania Calandrini[8], Marco Pettini[5,9], Sandra Ruffenach[2], Jeremie Torres[2,9]*

Electrodynamic interactions between biomolecules are of potential biological interest for temporal and spatial molecular controls, warranting investigation of their activation through various mechanisms in living systems. Using a light-harvesting protein in the phycobilisome antenna system of red algae, we proved that not only light exposure but also thermal energy alone can trigger attractive electrodynamic interactions up to hundreds of nanometers, sustained by low-frequency collective modes. Activation of such modes and interactions might influence conformational rearrangements and energy transport within the phycobilisome system. This paradigm shift underscores the immense potential of biological systems in exploiting different forms of energy to achieve optimal energy transfer.

INTRODUCTION

Nature has evolved a number of different strategies to maintain cellular homeostasis and ensure proper physiological functions (*1*, *2*). These strategies rely on a precise combination of temporal and spatial molecular controls, ensuring that molecular interactions occur at precise times and places. Living systems operate over a wide range of energy scales, from low-energy interactions (e.g., van der Waals forces, hydrogen bonding, and electrostatic interactions) to more specific high-energy interactions (e.g., covalent bonds and stereospecific interactions between macromolecular complexes). In this context, low-energy interactions appear to be crucial as they produce collective effects that are involved in the cohesion of intracellular compartmentalization. When they occur in the vicinity of critical phase transition conditions, these low-energy, weakly specific interactions lead to the formation of biocondensates (e.g., the formation of structures separated by a liquid-liquid phase in the cytoplasm) that serve as temporary storage or organizing centers for molecular activities (*3*). However, although conventional (quasi)electrostatic interactions are crucial (*4*) for short-range interactions, their effectiveness is limited both by the Debye screen in the crowded cellular environment and by the high permittivity values of water. To complete the picture, selective, long-range electrodynamic (ED) interactions must also be considered (*5*). These ED interactions resulting from external energy input above a certain threshold are sustained by giant oscillating electric dipoles induced by a nontrivial energy condensation into [subterahertz (sub-THz)] collective modes.

Experimental evidence for energy condensation into low-frequency collective modes at room temperature in open thermodynamic systems, where the energy is continuously transferred between biomolecules and their surroundings, has only recently been demonstrated (*6*, *7*). In addition, resonant dipole-dipole intermolecular ED forces, which act over long distances of several hundreds of angstroms and directly stemming from energy condensation, have been found (*8*) (see movie S1 for a general explanation). Consequently, there has been renewed interest in the field, either from a quantum mechanical point of view (*9*–*12*), with the terminology of phonon condensation, or from a (semi)classical perspective (*13*–*15*), in terms of collective oscillations/excitation, attracting a wide scientific audience spanning from (bio)physics (*16*) and technology (*17*, *18*) to biology (*19*, *20*), chemistry (*21*), and even quantum consciousness (*22*).

Here, using as model system R-phycoerythrin (R-PE), a light-harvesting protein naturally equipped with fluorochromes (see also fig. S1) sensitive to visible light (*23*), we have compared the sub-THz spectrum of R-PE protein in solution upon illumination with a 488-nm laser (i.e., protocol 1), with the one obtained without laser (i.e., protocol 2), both at increasing powers of the THz probe. To compensate for the thermal energy loss upon switching off the laser, the temperature in the second protocol has been adjusted in such a way as to match the temperatures achieved in the experiment with laser. The corresponding temperature ramp varies in the interval 20° to 29°C, which is below the protein denaturation temperature (thermal unfolding transitions at 56° and 72°C) (*24*, *25*). Although both experimental protocols feature a collective vibration at 73 GHz, a second collective vibration at 103 GHz is excited only upon laser illumination, after the saturation of the first mode. Because of the low frequency of the second mode, one could expect that it is always populated within the investigated temperature range, which is not the case. This suggests a nontrivial role of the electronic excitation of the protein fluorochromes in providing the protein with an additional path for energy transfer/dissipation at low frequency (103 GHz). Last, the observed frequency dependence of those modes on protein concentration proves that they are accompanied by the activation of ED forces between proteins over distances of several hundreds of angstroms.

RESULTS

Evidencing thermal activation of biomolecule collective oscillations

Under laser light illumination conditions (see Materials and Methods), when the laser power exceeds a threshold value, R-PE protein diluted

[1]Institut d'Electronique et des Systemes, University of Montpellier CNRS, Montpellier, France. [2]Laboratoire Charles Coulomb, University of Montpellier CNRS, Montpellier, France. [3]Institute of Applied Electrodynamics and Telecommunications, Vilnius University, Vilnius, Lithuania. [4]Micronit BV, Colosseum 15, 7521 PV Enschede, Netherlands. [5]Aix-Marseille Univ, Université de Toulon, CNRS, CPT, Marseille, France. [6]Department of Chemistry and Molecular Biology, University of Gothenburg, 40530 Göteborg, Sweden. [7]Centre d'Immunologie de Marseille Luminy, University of Aix-Marseille CNRS INSERM, Marseille, France. [8]Computational Biomedicine (IAS-5/INM-9), Institute for Advanced Simulation, Forschungszentrum Jülich, 52428 Jülich, Germany. [9]Quantum Biology Lab, Howard University, 16 17, Washington, DC 20059, USA.
*Corresponding author. Email: jeremie.torres@umontpellier.fr
†These authors contributed equally to this work.

in a phosphate-buffered saline (PBS) solution enters into a coherent vibrational state, exhibiting two distinct spectral resonances, as indicated by arrows in Fig. 1A (pink curve). These two resonances correspond to the fundamental mode (~73 GHz) and the second order mode (~103 GHz) of the collective oscillations of the R-PE protein, respectively. The frequencies of each of these modes are in agreement with previous experiments carried out on the same biological system with a different experimental setup (*8*). The high sensitivity and reliability of our THz biosensor enable precise temperature control throughout experimental procedures (see Materials and Methods), thus allowing the extraction of very faint THz signals from noise (fig. S1) (see the Supplementary Materials). To verify whether the excitation of such low-frequency vibrations can be explained in terms of simple thermal effects induced by the laser and the THz source (operated at 60 and 100 mW, respectively, and resulting in a measured temperature of 29°C in the sample), we performed an experiment without laser but fixing the temperature at 29° ± 0.05°C (purple curve in Fig. 1A). Notably, only the fundamental oscillation mode is excited, whereas the second-order mode is not sustained by thermal excitation. To further investigate the interplay between optical and thermal excitations, we run two sets of experiments, with and without laser, each at different THz source powers. The temperature of the setup without the laser is set in such a way as to match the corresponding steady-state temperature of the experiment with the laser. Figure 1B shows the corresponding normalized transmission spectra for optical excitation (solid lines) and thermal excitation (dashed lines) at different THz radiation powers. This systematic investigation further corroborates the fact that, whereas the fundamental mode at 73 GHz is excited in both experimental protocols, the second mode at 103 GHz can be activated only in the presence of light excitation. By increasing the THz power, which results in an effective temperature increase, the mode at 103 GHz is progressively populated, after a saturation effect on the mode at 73 GHz for a THz source power above 50 mW. In the experiment without light, an analogous increase in the THz power accompanied by temperature adjustment, to compensate for the loss of the laser thermal energy, does not result in the activation of the second collective vibration. Together, these experiments suggest that the excitation of the electronic degrees of freedom of the fluorochromes by laser light plays a fundamental role in making possible the excitation of the second collective mode at 103 GHz at room temperature. Upon light excitation, an additional efficient path for energy transfer into the low-frequency collective modes is available to the system.

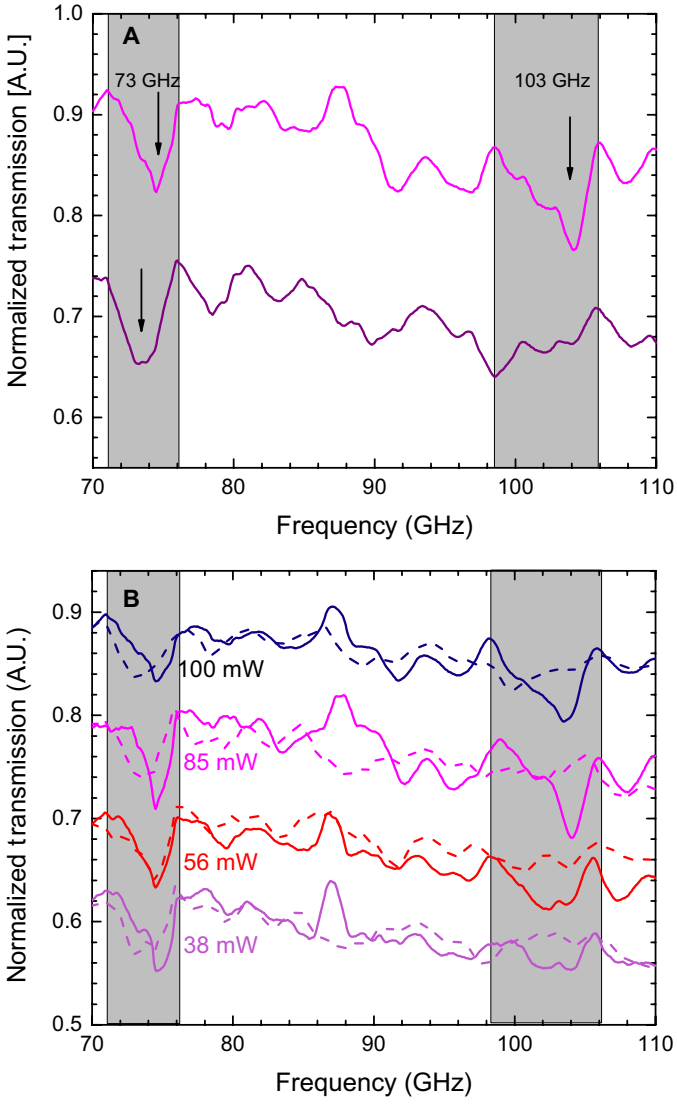

Fig. 1. Fingerprints of protein collective oscillations. (**A**) Protein solutions are excited by either laser light (pink) or thermal energy (purple). In both protocols, the protein concentration, *C*, is 7.2 μM and the THz source power is 100 mW. The laser power is 60 mW. The temperature in the thermal setup is fixed to 29°C, which matches the one achieved upon laser illumination (see Methods for more details). Collective oscillations at 73 and 103 GHz are indicated by arrows and highlighted in gray. (**B**) Normalized transmission spectra upon laser illumination (continuous line) or without laser (dashed line) with varying THz source power from 38 to 100 mW, all at $C = 4.0$ μM. Spectra without illumination are taken at temperatures matching those of the setup with the laser on (see Methods for more details). All spectra are vertically translated for clarity. A.U., arbitrary units.

The activation of collective intramolecular vibrations

Once established that the fundamental mode at 73 GHz can be thermally excited, the dependency of this collective vibration on temperature has been systematically studied in the range of 22° to 29°C with 0.5°C steps, for three different concentrations (Fig. 2, A, C, and E). Temperature was varied following a ramp with steps of 0.1°C (see temperature control in fig. S3). To ensure consistency, the averaged PBS buffer spectrum at 22°C is used as reference. The fundamental mode at 73 GHz is more and more populated as the temperature rises above a threshold value, until becoming fully excited, with its amplitude remaining constant upon further temperature increase. The temperature interval where this transition occurs matches the optimum temperature range for red algae growth (*26*), observed within a restricted temperature range of 20° to 28°C (*27*). Accordingly with the natural physiological conditions of red algae, temperature was identified as the principal physical determinant influencing the seasonal and latitudinal distribution of seaweed (*28*). Research conducted at Klein Oesterwal, Langebaan Lagoon, South Africa, revealed a positive correlation between the growth of red algae and elevated temperatures, with increased growth measurements recorded between 22° and 30°C and a decline in growth at 18°C (*29*). This temperature range is also very far below the thermal unfolding of R-PE protein (*24*).

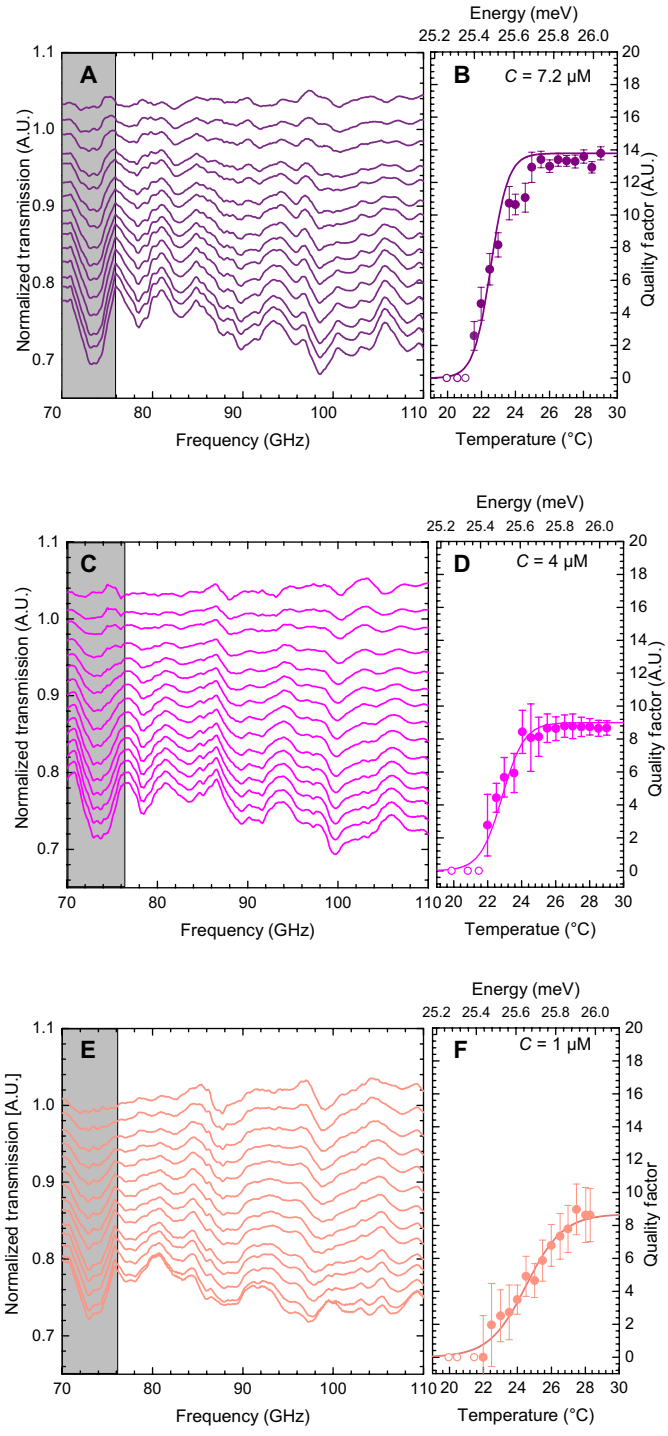

Fig. 2. Thermal activation of collective oscillations (concentration dependent). In all panels, the temperature varies from 22°C (top) to 29°C (bottom) with 0.5°C steps, whereas the laser is off and the THz source power is set to 100 mW. (**A**) THz transmission spectra of R-PE protein at $C = 7.2$ μM normalized to averaged PBS buffer spectra at 22°C. Gray area marks the fundamental mode zone used to extract the *Q*-factor. (**B**) Fundamental mode *Q*-factor dependence with temperature at $C = 7.2$ μM. The threshold-like behavior characteristic of a phase transition is highlighted by the continuous line. Same at $C = 4.0$ μM (**C** and **D**) and at $C = 1.0$ μM (**E** and **F**). Open circles are set to zero. Error bars were estimated using the SD coefficient multiplied by a concentration dependent factor to overestimate the errors at low concentrations. All spectra are vertically translated for clarity.

Notably, for all the investigated concentrations, the variation of the quality factor *Q* indicates that the saturation of the fundamental mode follows a threshold-like behavior (Fig. 2, B, D, and F). This feature resembles a nonequilibrium phase transition; when the energy input rate exceeds a critical value, thermal energy is channeled by the system into this coherent oscillation. Even if this behavior has been previously reported for proteins subjected to light excitation (*8*), this phase transition–like behavior induced by the increase in temperature alone has never been reported before.

For the investigated protein concentrations, the transition from unexcited to fully excited collective oscillation occurs at ~4°C, i.e., with an extra energy above the threshold temperature of ~0.3 meV (see also fig. S4). Notably, there is a slight decrease in the threshold temperature as the concentration increases, and the *Q*-factor values in the concentration range of 1.0 to 6.0 μM are almost half of the one at 8.0 μM. The threshold is also more abrupt in the latter cases. Drawing an analogy with (collective) spontaneous emission (Schawlow-Townes law) or super-radiance mechanism (*30*–*33*), the *Q*-factor increase with increasing concentration is consistent with the picture that the number of proteins involved in the in-phase collective oscillation also increases, this behavior being also reproduced under the laser light excitation protocol (fig. S5). The observation that, at lower protein concentrations, a higher energy input is required to initiate the collective oscillation suggests a possible cooperative effect between proteins.

Thermally activated long-range ED interaction

Figure 3A shows the normalized transmission THz spectra for different concentrations, subjected to optical (solid lines) or thermal (dashed lines) excitation. For a direct comparison, the thermal excitation spectra are provided at temperatures equivalent to those produced by laser light excitation. As previously remarked, the fundamental mode at ~73 GHz can be excited in both cases, whereas the second mode at ~103 GHz is excited only upon laser light illumination (starting from a protein concentration of 1.0 μM). The slight discrepancy in the fundamental mode frequency between the two excitation processes can be attributed to possibly different states explored by the proteins during these excitation processes. Figure 3B also depicts the normalized transmission THz spectra at different concentrations as obtained solely through thermal excitation at temperature at which the fundamental mode is fully populated regardless of concentration. After extracting the dependency of the fundamental mode frequency ν on concentration, we report the corresponding normalized frequency shift variation $\Delta\nu = \nu - \nu_0$ versus the average intermolecular distance, ν_0 being the unperturbed frequency at infinite dilution, i.e., $< r > \rightarrow +\infty$ (Fig. 3C). The fundamental mode frequency shifts, both for optical (orange circles) and thermal (purple squares) excitation, are found to be inversely proportional to the cube of the intermolecular average distance. This serves as a proof of concept for the thermal activation of long-range ED attractive and selective forces, which is consistent with our classical version of the Fröhlich hypothesis (*13*). In this scenario, the proteins are all in a collective oscillation state, leading to the activation of long-range ED forces over distances up to $< r > \sim 1350$ Å, upon thermal activation, and ~1750 Å, upon laser light excitation. It is thus clear that light is more efficient at activating intermolecular forces because the damping of the fundamental collective oscillation within this excitation mechanism is lower than in the thermal one. Experimental data have been fitted with a power law of the form $\Delta\nu/\nu_0 = A < r >^{-3}$, where A is a real number. For thermal excitation, $A = 2.60 \times 10^6$ Å^3

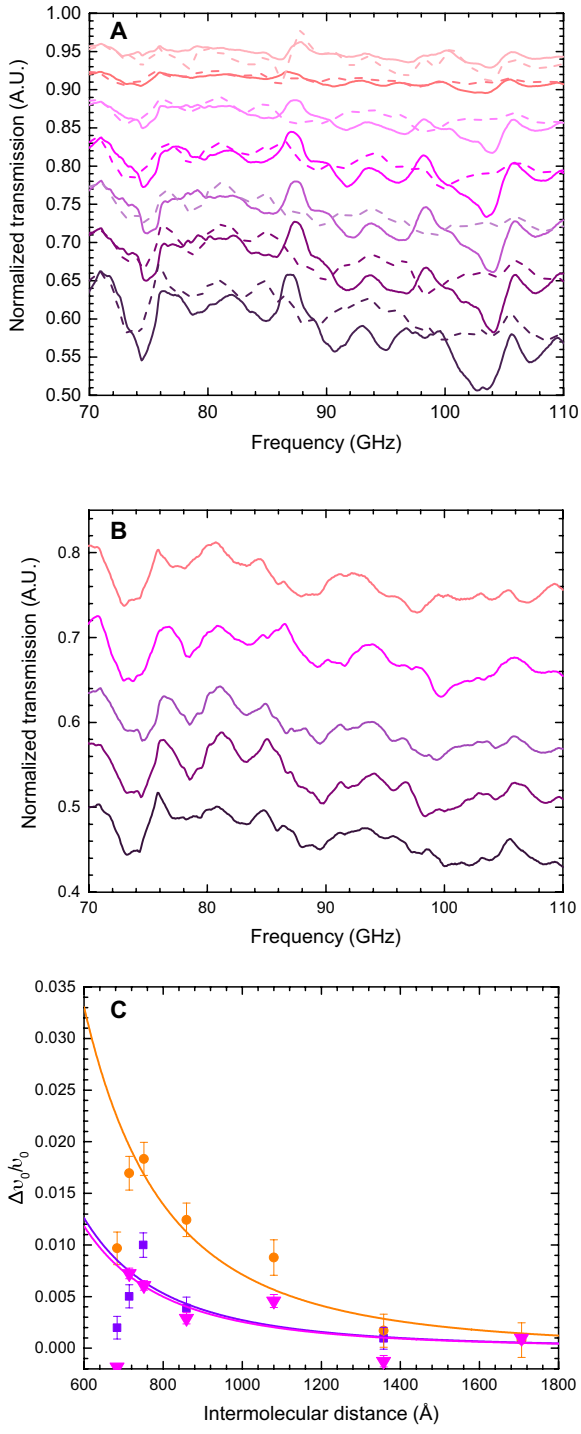

Fig. 3. Thermal activation of ED forces. (**A**) Normalized transmission spectra with varying protein concentration. From top to bottom: $C = 0.5$, 1.0, 2.0, 4.0, 6.0, 7.2, and 8.0 μM. Solid lines: laser light excitation protocol (laser power = 60 mW). Dashed lines: thermal excitation protocol (laser off and the temperature at each concentration is adjusted to match the temperature achieved in the corresponding laser light excitation setup). (**B**) Normalized transmission spectra with varying protein concentration at a fixed excitation temperature of $T = 28$°C (thermal excitation protocol). Spectra are vertically translated for clarity. (**C**) Frequency shift dependence to intermolecular distance for the fundamental mode upon thermal excitation at $T = 28$°C (purple squares) and the fundamental mode (orange circles) and the second mode (pink triangles) upon optical excitation. For all, THz power is set at 100 mW.

whereas for laser excitation, $A = 7.14 \times 10^6$ Å^3, in good agreement with theoretical expectations (*8*). This increase in A might be related to the enhancement in the oscillation amplitude, which entails a larger oscillating dipole moment, consistent with the increase in Q values with laser light excitation (fig. S5). Consequently, this results in stronger intermolecular ED interactions and a larger frequency shift for a given distance (i.e., concentration). The larger strength of ED interactions generated by light could also be related to some protein conformational changes upon light illumination at high concentrations, as further supported by circular dichroism experiments (table S1). At low concentrations (large interprotein distance), the peak depicting the fundamental mode shows a similar frequency in both excitation experimental protocols, whereas a progressive frequency shift is observed at higher concentrations (fig. S6). However, laser light activation of ED interactions, supported by giant collective oscillations, remains a reversible mechanism (fig. S7), suggesting that any subunit of a phycobilisome can be quenched and light-controlled switches are activated to intrinsically available energy-dissipating states (*34*–*36*). At high concentrations, as clearly illustrated in Fig. 3C, the data point at 684 Å (corresponding to 8 μM) does not follow the expected tendency, which is entirely understandable considering that a conformational changes in the protein are observed at concentrations above 6 μM (see fig. S5 and table S1) even if denatured R-PE subunits remain photosensitive (*37*). Last, we note that also the frequency shift of the mode at ~103 GHz (optical setup) as a function of the average interprotein distance (Fig. 3C, pink triangles) shows an $< r >^{-3}$ dependence ($A = 2.55 \times 10^6$ Å^3), thus suggesting a further source of ED interactions sizably active over distances up to $< r > \sim 1750$ Å.

DISCUSSION

The reported experiments provide a proof of concept for the possible activation, by means of thermal energy alone, of attractive long-range ED intermolecular interactions up to ~1350 Å, correlated to the excitation of collective (coherent) low-frequency vibrations of the protein at ~73 GHz. Although we could not clarify whether the excitation of such collective low-frequency vibrations is accompanied by an energy condensation phenomenon as hypothesized by Fröhlich (*5*), i.e., by a redistribution of the energy from the high-frequency modes to the lowest frequency one, the corresponding Q-factor features a typical phase transition–like evolution when the temperature rises above a threshold value. Furthermore, the Q-factor evolution with protein concentration increase is compatible with the occurrence of in-phase collective oscillations, i.e., with the synchronization of the oscillators in the sample, which results in enhanced dipole moment fluctuations.

The mechanisms behind the activation of coherent oscillations and attractive "giant dipoles" upon excitation by "disordered" thermal energy remain elusive. Water restructurings at the water-protein interface, i.e., the dynamic exchange between free and bound water species and the strength of the hydrogen bonds (*38*), might play a role. Recently, it has been proposed that sub-THz electromagnetic fields could, by reducing the orientational polarization of water molecules at the interface, decrease the dielectric permittivity of a lysozyme solution (*18*). In (*39*), anisotropic heat transfer from solvent through a protein has been discussed for soybean lipoxygenase (SLO) enzyme, a prototypical thermally activated enzyme. Specifically, it has been proved that SLO's catalytic activity involves quantum mechanical tunneling of a hydrogen

atom from the substrate to the active site cofactor, which critically depends on the thermal activation of the protein scaffold. Collisions between water and a solvent-exposed loop initiate thermal activation at the protein surface that is then propagated toward the reactive site through a discrete thermal network within the protein (*20*). Analogous thermal activation has been reported for thermophilic alcohol dehydrogenase (*40*). Such anisotropic networks provide an efficient route for productive heat transfer in thermally activated enzyme reactions (*20*). The impact of thermal excitation has also been investigated in self-organized processes such as tubulin polymerization (*41*). Microtubules growth distortion upon exposure to microwave radiation, infrared laser, or hot air turns out to be independent of the external excitation process as long as the corresponding thermal history is the same. Also in R-PE protein, both thermal and optical excitations can activate the same low-frequency mode at 73 GHz when operated under equivalent temperature conditions. Conversely, the second mode at 103 GHz appears only upon laser excitation. These findings suggest that, whereas the activation of the first vibrational mode can be related to a pure thermal effect, the second one indicates a nontrivial role of the electronic excitation of the protein fluorochromes in allowing the protein to tunnel the absorbed energy into this additional low-frequency vibrational mode.

The energy conversion pathway going from the electronic excitation of the fluorochromes until the activation of such low-frequency modes is an intrinsically multiscale problem both in time and space. Many papers have addressed the role of intramolecular charge transfer and vibronic excitons of the chromophores to explain energy transfer mechanisms in light-harvesting proteins [see, for instance, (*42*–*45*)]. Here, we provide the experimental evidence that light plays a key role in the activation of a specific collective mode at very low-frequency collective modes at (103 GHz). The corresponding frequency shift with protein concentration indicates that attractive long-range (up to ~1750 Å) ED interactions are, in turn, activated. However, whereas in a previous study (*8*), we demonstrated that such ED forces lead to the formation of molecular clusters; the accurate description of such out-of-equilibrium systems, which are in constant evolution, remains a notable scientific challenge (*46*, *47*). Buffers and water might play a crucial role in sustaining collective oscillations of proteins (*48*). To address this topic, a natural follow-up of this research would be the investigation of the effect of cosolvents able to modify water polarizability and viscosity.

Last, being out-of-equilibrium conditions ubiquitous in living systems, thermal activation of long-range ED interactions sustained by collective vibrations may help into the context of more general mechanisms such as molecular cascade of events. This insight alters the perspective on how concentration might affect chemical potential and may influences biomolecular reaction rates, in both in vitro and in vivo environments. Although increasing the concentration of noninteracting molecules can raise the frequency of productive random collisions, potentially enhancing reaction rates, our findings suggest that other concentration-dependent factors, such as ED forces, may also drive the assembly and conformational changes of biological macromolecules.

MATERIALS AND METHODS

Sample preparation

The R-PE is composed of an αβ-hexamer (αβ)6γ structure. Each α subunit contains two phycoerythrobilins, the β subunit contains three phycoerythrobilins and one phycourobilin, and the γ subunit contains two or three phycoerythrobilins and one or two phycourobilins. This arrangement allows for some variability in the number of fluorochromes, typically around 38 (fig. S1A). R-PE exhibits one of the most intense fluorescence signals among all known fluorescent dyes. The pigments in R-PE are highly responsive to light with a wavelength of 488 nm, which was used in these experimental investigations (fig. S1B).

R-PE was purchased from Antibodies.com Europe AB with ref. A269981. PBS and Slide-A-Lyzer 10K MWCO dialysis cassettes were purchased from Thermo Fisher Scientific. R-PE was prepared by dialyzing ≈1.4 ml of stock protein (~31 mg) against 500 to 700 ml of PBS at 4°C for 2 hours with continuous stirring and then, after exchanging PBS, for overnight at 4°C and stored at 4°C in PBS.

Design and fabrication of integrated THz biosensors

The THz biosensor specially developed for the experiments is made up of a microfluidic cartridge and a THz electronic system, assembled together with a special clamping platform from Micronit BV. This platform ensures that the protein solution flows through the cuvette (fig. S2A).

The electronic system includes a highly efficient THz detector based on silicon field-effect transistors developed by the Taiwan Semiconductor Manufacturing Company (TSMC). It features a spiral antenna that covers the 0.1- to 0.3-THz frequency band. Together with its readout circuit, this forms a so-called "rectenna." A 500-μm-thick silicon plate is mounted under the chip to position a silicon hyperhemispherical lens (about 12 mm in diameter). This technology was chosen to create low-cost biosensors that can work with proteins of different masses and resonances signatures appearing across a wide frequency range. A typical photoconductivity response from the THz electronic system alone is shown in fig. S2B.

The microfluidic platform effectively addresses the major challenge of THz absorption by water with a well-designed microcuvette that is a few tenths of the wavelength (fig. S2C). However, developing this platform requires careful selection of materials and structures as they widely affect bandwidth, frequency resolution, signal-to-noise ratio, and dynamic range of measurements (*49*). The materials used should have low absorption characteristics at THz frequencies and be suitable for low-cost processing techniques. Suitable materials include cyclic olefin polymer (COP), high-density polyethylene, polystyrene, and quartz, although quartz is challenging to process. Polydimethylsiloxane is also a good option due to its excellent molding properties, despite higher THz absorption. We chose a COP that balances low cost, short processing time, transparency in the frequency band of interest (fig. S2C), and the ability to be machined to the desired characteristics. A wide serpentine (fig. S2D) filled with pure water is used to absorb unwanted THz radiation.

Last, a second silicon-based hemispheric lens efficiently couples the THz beam into the electronic system, whereas proteins lying in the microfluidic cuvette are excited by either a 488-nm laser or a thermal heater. This setup protects the electronic system from potential damage caused by the protein solution and improves stability and reliability by keeping the THz system at a constant temperature, unaffected by the blue light and heat from the protein bath.

Metrology of temperature control

All experiments were conducted at room temperature to maintain consistent conditions throughout the study. The biosensor's

temperature regulation relies on two key components: a thermal bath surrounded by a heating foil and a microthermocouple. The thermal bath, positioned directly on top of the microfluidic chip, ensures efficient thermal conduction and indirectly heats the microfluidic chip. A proportional-integral-derivative controller precisely regulates the temperature, maintaining a precision of ±0.1°C. The microthermocouple, placed as close as possible to the microfluidic chip, allows for real-time temperature monitoring. Moreover, because the water absorption in the THz frequency range is temperature dependent and because the laser illumination caused a slight increase in the thermal bath temperature, especially when the protein is immersed into the buffer, we have characterized the dependence of amplitude on temperature for several frequency bands ranging from 60 to 120 GHz with a 5-GHz step (fig. S3A) over almost 10 hours of experiments. As expected, the bands follow the temperature variation (shown in red) of the thermal bath during an experiment. Thus, we implemented a temperature regulation on the biosensor. To control and monitor the thermal bath temperature, a heating foil and a microthermocouple were respectively installed as close as possible to the chips, inside the cuvettes of both experiments. In addition, changes in ambient temperature were monitored using a ThorLabs TSP01-USB DataLogger with an negative temperature coefficient (NTC) probe. This temperature and humidity probe, equipped with a USB interface, allowed real-time monitoring of room temperature changes. Temperature control stability of the thermal bath for an incident radiation of 90 GHz is plotted in fig. S3B. A control of 1 mV of THz-induced photoconductivity by 0.1°C was thus obtained.

The metrology of the biosensor was assessed by measuring the variation in spectra amplitude over 15 scans (equivalent to 1350 s) and by ensuring accuracy with temperature fluctuations or deviations. Figure S2E thus illustrates the reproducibility of THz spectrums with temperature regulation at $T = 22$°C measured in the buffer of reference (PBS) with temperature regulation. The spectrums obtained with the biosensor demonstrate a typical relative deviation in percent of ±0.25%.

THz spectroscopy protocol

The continuous wave THz radiation (WR10 waveguide) was generated using a Signal Generator Extension (SGX) module from Virginia Diodes Inc. The averaged power over the recommended frequency band (70 to 110 GHz) was ~100 mW (20 dBm). For optical excitation, a Spectra Physics blue laser (Excelsior One 488C-50) was emitting at 488 nm and delivering a maximum power of 50 mW. This wavelength was selected because it provided sufficient energy to put the proteins under out-of-equilibrium conditions. The output power was controlled by a series of optical density filters, allowing for precise adjustment of the optical power density. It is worth noting that, whereas each measurement was at least two or three times reproduced (fig. S8), showing similar responses and indicating robust results [data availability at (*50*)]. Averaging these measurements was so avoided as averaging could introduce significant errors and mask the true protein response due to slight variations under experimental conditions and potential protein degradation over time. This approach prevents misrepresentation of the actual protein behavior under nonequilibrium conditions.

Protocols for THz spectroscopy experiments

Thermal excitation prior to laser excitation. The protocol followed for thermal excitation before laser excitation can be summarized in five steps:

1) Fast ramp from room temperature (usually 19°C) up to 22°C during 15 min.

2) Checking the system stabilization in temperature by verifying a normalized signal amplitude variation of less than 1% for at least 10 consecutive THz scans (~15 min) at 22°C.

3) Ramp up to high temperature (29°C for $C < 4$ μM and 33°C for $C > 4$ μM). THz spectrums are acquired during a temperature ramp with an average rate of ≈0.4 hours/°C). This allows us to determine the equivalent temperature (T_{eq}), i.e., the variation of temperature induced by the laser, for each frequency and for each concentration, by comparing those measurements with those obtained with optical excitation (see below).

4) Then, a slow temperature decrease up to 22°C to control any discrepancies between before/after temperature ramp.

5) Last, we repeat the second step, recording at least 10 consecutive THz scans at 22°C with a normalized signal variation of less 1%. The average of those scans is used as reference for normalization procedure.

Optical excitation. Just after thermal excitation, the optical excitation is carried out in a single step: Spectra are acquired once the laser is turned on during 45 min of illumination.

Thermal excitation post-laser excitation. Last, immediately after optical excitation, we proceed to reanalyze the thermal stability of the system. Specifically, this process can be divided into three parts:

1) First, right after switching off the laser, 10-THz scans are acquired for a duration of ~15 min.

2) Follows a rest period of 45 min, also named dark period, during which both laser and THz radiations are turned off.

3) Next, 10-THz spectra are acquired once the THz radiation is turned on again to check the reversibility of the process and as a first step to discriminate proteins spectral fingerprints from experimental artifacts.

Data analysis and normalization procedure

A THz normalized transmission spectra consists of the division of the spectra at a defined temperature for thermal excitation and at a define time of illumination for the optical excitation by the average obtaining at 22°C without illumination (step 5 in thermal excitation prior to laser excitation). An average of the data with 15 window points is performed as smoothing.

Supplementary Materials

The PDF file includes:

Figs. S1 to S8
Table S1
Legend for movie S1

Other Supplementary Material for this manuscript includes the following:

Movie S1

REFERENCES AND NOTES

1. H. Kitano, Biological robustness. *Nat. Rev. Genet.* **5**, 826–837 (2004).
2. B. Alberts, A. Johnson, J. Lewis, M. Raff, K. Roberts, P. Walter, "The mitochondrion" in *Molecular Biology of the Cell* (Garland Science, 2002).
3. R. V. Pappu, S. R. Cohen, F. Dar, M. Farag, M. Kar, Phase transitions of associative biomacromolecules. *Chem. Rev.* **123**, 8945–8987 (2023).
4. M. Poudyal, K. Patel, L. Gadhe, A. S. Sawner, P. Kadu, D. Datta, S. Mukherjee, S. Ray, A. Navalkar, S. Maiti, D. Chatterjee, J. Devi, R. Bera, N. Gahlot, J. Joseph, R. Padinhateeri, S. K. Maji, Intermolecular interactions underlie protein/peptide phase separation irrespective of sequence and structure at crowded milieu. *Nat. Commun.* **14**, 6199 (2023).
5. H. Fröhlich, Long-range coherence and energy storage in biological systems. *Int. J. Quantum Chem.* **2**, 641–649 (1968).

6. I. V. Lundholm, H. Rodilla, W. Y. Wahlgren, A. Duelli, G. Bourenkov, J. Vukusic, R. Friedman, J. Stake, T. Schneider, G. Katona, Terahertz radiation induces non-thermal structural changes associated with Fröhlich condensation in a protein crystal. *Struct. Dyn.* **2**, 054702 (2015).
7. I. Nardecchia, J. Torres, M. Lechelon, V. Giliberti, M. Ortolani, P. Nouvel, M. Gori, Y. Meriguet, I. Donato, J. Preto, L. Varani, J. Sturgis, M. Pettini, Out-of-equilibrium collective oscillation as phonon condensation in a model protein. *Phys. Rev. X* **8**, 031061 (2018).
8. M. Lechelon, Y. Meriguet, M. Gori, S. Ruffenach, I. Nardecchia, E. Floriani, D. Coquillat, F. Teppe, S. Mailfert, D. Marguet, P. Ferrier, L. Varani, J. Sturgis, J. Torres, M. Pettini, Experimental evidence for long-distance electrodynamic intermolecular forces. *Sci. Adv.* **8**, eabl5855 (2022).
9. Z. Zhang, G. S. Agarwal, M. O. Scully, Quantum fluctuations in the Fröhlich condensate of molecular vibrations driven far from equilibrium. *Phys. Rev. Lett.* **122**, 158101 (2019).
10. Y. Wang, Y. Wang, F. Hu, L. Zeng, Z. Chen, M. Jiang, S. Lin, W. Guo, D. Li, Surface-functionalized terahertz metamaterial biosensor used for the detection of exosomes in patients. *Langmuir* **38**, 3739–3747 (2022).
11. A. A. Svidzinsky, L. Yuan, M. O. Scully, New kind of condensation of bose particles through stimulated processes. *J. Low Temp. Phys.* **208**, 184–195 (2022).
12. K. Sasihithlu, G. D. Scholes, Vibrational dipole–dipole coupling and long-range forces between macromolecules. *J. Phys. Chem. B* **128**, 1205–1208 (2024).
13. J. Preto, M. Pettini, J. A. Tuszynski, Possible role of electrodynamic interactions in long-distance biomolecular recognition. *Phys. Rev. E* **91**, 052710–052728 (2015).
14. B. A. Tay, Excitation relaxation in a molecular chain and energy transfer at steady state. *Phys. Rev. E* **103**, 042124 (2021).
15. A. Tenenbaum, Energy condensation and dipole alignment in protein dynamics. *Phys. Rev. E* **109**, 044401 (2024).
16. K. Azizi, M. Gori, U. Morzan, A. Hassanali, P. Kurian, Examining the origins of observed terahertz modes from an optically pumped atomistic model protein in aqueous solution. *PNAS Nexus* **2**, pgad257 (2023).
17. X. Zheng, B. Li, Fröhlich condensate of phonons in optomechanical systems. *Phys. Rev. A* **104**, 043512 (2021).
18. J. Sugiyama, Y. Tokunaga, M. Hishida, M. Tanaka, K. Takeuchi, D. Satoh, M. Imashimizu, Nonthermal acceleration of protein hydration by sub-terahertz irradiation. *Nat. Commun.* **14**, 2825 (2023).
19. V. N. Kadantsev, A. Goltsov, Collective excitations in α-helical protein structures interacting with the water environment. *Electromagn. Biol. Med.* **39**, 419–432 (2020).
20. J. P. T. Zaragoza, A. R. Offenbacher, S. Hu, C. L. Gee, Z. M. Firestein, N. Minnetian, Z. Deng, F. Fan, A. T. Iavarone, J. P. Klinman, Temporal and spatial resolution of distal protein motions that activate hydrogen tunneling in soybean lipoxygenase. *Proc. Natl. Acad. Sci. U.S.A.* **120**, e2211630120 (2023).
21. A. V. Stepanov, M. A. Stepanov, Negative entropy production in L-lactate dehydrogenase kinetics. *Arch. Biochem.* **6**, 001–009 (2023).
22. J. R. Reimers, L. K. McKemmish, R. H. McKenzie, A. E. Mark, N. S. Hush, Weak, strong, and coherent regimes of Fröhlich condensation and their applications to terahertz medicine and quantum consciousness. *Proc. Natl. Acad. Sci. U.S.A.* **106**, 4219–4224 (2009).
23. C. Contreras-Martel, J. Martinez-Oyanedel, M. Bunster, P. Legrand, C. Piras, X. Vernede, J. C. Fontecilla-Camps, Crystallization and 2.2 Å resolution structure of R-phycoerythrin from Gracilaria chilensis: A case of perfect hemihedral twinning. *Acta Crystallogr. D Biol. Crystallogr.* **57**, 52–60 (2001).
24. A. Simovic, S. Combet, T. C. Velickovic, M. Nikolic, S. Minic, Probing the stability of the food colourant R-phycoerythrin from dried Nori flakes. *Food Chem.* **374**, 131780 (2022).
25. N. Senthilkumar, C. Kurinjimalar, R. Thangam, V. Suresh, G. Kavitha, P. Gunasekaran, R. Rengasamy, Further studies and biological activities of macromolecular protein R-Phycoerythrin from *Portieria hornemannii*. *Int. J. Biol. Macromol.* **62**, 107–116 (2013).
26. S. P. Singh, P. Singh, Effect of temperature and light on the growth of algae species: A review. *Renew. Sustain. Energy Rev.* **50**, 431–444 (2015).
27. M. Fethi, A. B. Ghedifa, Optimum ranges of combined abiotic factor for Gracilaria gracilis aquaculture. *J. Appl. Phycol.* **31**, 3025–3040 (2019).
28. R. Mouedden, S. Abdellaoui, F. El Madani, N. El Ouamari, D. Slimani, K. Kasmi, M. Taibi, I. Zahir, K. Chaabane, *Gracilaria Gracilis*—A review of ecological knowledge, chemical composition, cultivation, and applications. *Ecol. Eng. Environ. Technol.* **25**, 276–287 (2024).
29. M. Beltrand, A. Dineen, C. Hitzeroth, B. Baum, C. De Cerff, C. De Vos, J. Lewis, S. Zaroufis, D. Pillay, Warming effects on two autogenic engineers (Zostera capensis and Gracilaria gracilis): Consequences for macrofaunal assemblages and benthic heterogeneity in intertidal sandflat ecosystems. *Estuaries Coast.* **45**, 247–259 (2022).
30. G. Grynberg, A. Aspect, F. Claude, *Introduction Aux Lasers et à l'optique Quantique* (Ellipses, 1997). [Introduction to Lasers and Quantum Optics].
31. R. H. Dicke, Coherence in spontaneous radiation processes. *Phys. Rev.* **93**, 99–110 (1954).
32. M. Gross, S. Haroche, Superradiance: An essay on the theory of collective spontaneous emission. *Phys. Rep.* **93**, 301–396 (1982).
33. N. S. Babcock, G. Montes-Cabrera, K. E. Oberhofer, M. Chergui, G. L. Celardo, P. Kurian, Ultraviolet superradiance from mega-networks of tryptophan in biological architectures. *J. Phys. Chem. B* **128**, 4035–4046 (2024).
34. M. Gwizdala, R. Berera, D. Kirilovsky, R. Van Grondelle, T. P. J. Krüger, Controlling light harvesting with light. *J. Am. Chem. Soc.* **138**, 11616–11622 (2016).
35. M. Gwizdala, T. P. J. Krüger, M. Wahadoszamen, J. M. Gruber, R. Van Grondelle, Phycocyanin: One complex, two states, two functions. *J. Phys. Chem. Lett.* **9**, 1365–1371 (2018).
36. M. Wahadoszamen, T. P. J. Krüger, A. M. Ara, R. Van Grondelle, M. Gwizdala, Charge transfer states in phycobilisomes. *Biochim. Biophys. Acta Bioenerg.* **1861**, 148187 (2020).
37. A. Vásquez-Suárez, F. Lobos-González, A. Cronshaw, J. Sepúlveda-Ugarte, M. Figueroa, J. Dagnino-Leone, M. Bunster, J. Martínez-Oyanedel, The γ33 subunit of R-phycoerythrin from Gracilaria chilensis has a typical double linked phycourobilin similar to γ subunit. *PLOS ONE* **13**, e0195656 (2018).
38. N. Nandi, B. Bagchi, Dielectric relaxation of biological water. *J. Phys. Chem. B* **101**, 10954–10961 (1997).
39. J. P. T. Zaragoza, A. Nguy, N. Minnetian, Z. Deng, A. T. Iavarone, A. R. Offenbacher, J. P. Klinman, Detecting and characterizing the kinetic activation of thermal networks in proteins: Thermal transfer from a distal, solvent-exposed loop to the active site in soybean lipoxygenase. *J. Phys. Chem. B* **123**, 8662–8674 (2019).
40. A. Kohen, R. Cannio, S. Bartolucci, J. P. Klinman, Enzyme dynamics and hydrogen tunnelling in a thermophilic alcohol dehydrogenase. *Nature* **399**, 496–499 (1999).
41. G. Hyammarin, P. Norder, R. Harimoorthy, G. Chen, P. Bernsten, P. O. Widlund, C. Stoij, H. Rodilla, J. Swenson, G. Bräden, R. Neutze, No observable non-thermal effect of microwave radiation on the growth of microtubules. *Sci. Rep.* **14**, 1826 (2024).
42. J. M. Womick, A. M. Moran, Vibronic enhancement of exciton sizes and energy transport in photosynthetic complexes. *J. Phys. Chem. B* **115**, 1347–1356 (2011).
43. W. F. Beck, Intramolecular charge transfer and the function of vibronic excitons in photosynthetic light harvesting. *Photosynth. Res.* **162**, 139–156 (2024).
44. S. Sil, R. W. Tilluck, N. Mohan T. M., C. H. Leslie, J. B. Rose, M. A. Domínguez-Martín, W. Lou, C. A. Kerfeld, W. F. Beck, Excitation energy transfer and vibronic coherence in intact phycobilisomes. *Nat. Chem.* **14**, 1286–1294 (2022).
45. E. A. Arsenault, Y. Yoneda, M. Iwai, K. K. Niyogi, G. R. Fleming, Vibronic mixing enables ultrafast energy flow in light-harvesting complex II. *Nat. Commun.* **11**, 1460 (2020).
46. M. A. Domínguez-Martín, P. V. Sauer, H. Kirst, M. Sutter, D. Bína, B. J. Greber, E. Nogales, T. Polívka, C. A. Kerfeld, Structures of a phycobilisome in light-harvesting and photoprotected states. *Nature* **609**, 835–845 (2022).
47. R. Moya, A. C. Norris, T. Kondo, G. S. Schlau-Cohen, Observation of robust energy transfer in the photosynthetic protein allophycocyanin using single-molecule pump–probe spectroscopy. *Nat. Chem.* **14**, 153–159 (2022).
48. S. K. Pandey, M. Cifra, Tubulin vibration modes are in the subterahertz range, and their electromagnetic absorption is affected by water. *J. Phys. Chem. Lett.* **15**, 8334–8342 (2024).
49. S. Alfihed, J. F. Holzman, I. G. Foulds, Developments in the integration and application of terahertz spectroscopy with microfluidics. *Biosens. Bioelectron.* **165**, 112393 (2020).
50. E. Pérez-Martín, Unveiling long-range forces in light harvesting proteins: Pivotal roles of temperature and light, Zenodo (2025); https://doi.org/10.5281/ZENODO.15045913.

Acknowledgments: We thank the Terakalis Company (terakalis.com) for support in designing the adaptation and holder for the Si lenses and the BioCampus Montpellier platform (https://biocampus.cnrs.fr/index.php/fr/) for circular dichroism experiments. **Funding:** This work was supported by the Terahertz Occitanie Platform and has received funding from the European Union's Horizon 2020 Research and Innovation Programme under grant agreement no. 964203 (FET-Open LINkS project) and by the French national funding agency through PEPR Electronique, axis COMPTERA no. LS263039. A.L. and K.I. acknowledge funding received from the Research Council of Lithuania (project no. SMIP-22-83). **Author contributions:** Conceptualization: V.C., T.B., L.B., F.T., E.P.-M., G.K., J.T., S.R., M.P., E.F., and D.M. Methodology: T.B., L.B., E.V., J.T., S.R., M.P., E.F., and D.M. Software: L.B. and S.R. Validation: L.B., E.P.-M., J.T., and S.R. Formal analysis: L.B., E.P.-M., and S.R. Investigation: L.B. and E.P.-M. Resources: T.B., L.B., A.L., F.T., E.V., K.I., and D.M. Data curation: E.P.-M. Writing—original draft: V.C., F.T., J.T., M.P., and E.F. Writing—review and editing: E.P.-M., J.T., and D.M. Visualization: E.V., E.P.-M., A.L., L.B., and J.T. Supervision: E.V., G.K., D.M., V.C., M.P. and J.T. Project administration: E.V., G.K., D.M., V.C., M.P. and J.T. Funding acquisition: V.C., A.L., G.K., J.T., S.R., K.I., M.P., E.F., and D.M. **Competing interests:** The authors declare that they have no competing interests. **Data and materials availability:** All data needed to evaluate the conclusions in the paper are present in the paper and/or the Supplementary Materials. All the details to reproduce the experimental outcomes and rough data are available in the Supplementary Materials.

Submitted 2 December 2024
Accepted 25 March 2025
Published 30 April 2025
10.1126/sciadv.adv0346